ACS APPLIED MATERIALS & INTERFACES

www.acsami.org

Research Article

Exploring the Membrane-Active Interactions of Antimicrobial Long-Chain Fatty Acids Using a Supported Lipid Bilayer Model for Gram-Positive Bacterial Membranes

Sungmin Shin, Jingyeong Yu, Hyunhyuk Tae, Yilin Zhao, Dongping Jiang, Yuan Qiao, Wooseong Kim, and Nam-Joon Cho*

Cite This: *ACS Appl. Mater. Interfaces* 2024, 16, 56705−56717

Read Online

ACCESS | Metrics & More | Article Recommendations | Supporting Information

ABSTRACT: The dynamic nature of bacterial lipid membranes significantly impacts the efficacy of antimicrobial therapies. However, traditional assay methods often fall short in replicating the complexity of these membranes, necessitating innovative approaches. Herein, we successfully fabricated model bacterially supported lipid bilayers (SLBs) that closely mimic the characteristics of Gram-positive bacteria using the solvent-assisted lipid bilayer (SALB) technique. By employing a quartz crystal microbalance with dissipation and fluorescence microscopy, we investigated the interactions between these bacterial mimetic membranes and long-chain unsaturated fatty acids. Specifically, linolenic acid (LNA) and linoleic acid (LLA) demonstrated interaction behaviors correlated with the critical micelle concentration (CMC) on Gram-positive membranes, resulting in membrane remodeling and removal at concentrations above their respective CMC values. In contrast, oleic acid (OA), while showing similar membrane remodeling patterns to LNA and LLA, exhibited membrane insertion and CMC-independent activity on the Gram-positive membranes. Particularly, LNA and LLA demonstrated bactericidal effects and promoted membrane permeability and ATP leakage in the bacterial membranes. OA, characterized by a CMC-independent activity profile, exhibited potent bactericidal effects due to its robust penetration into the SLBs, also enhancing membrane permeability and ATP leakage. These findings shed light on the intricate molecular mechanisms governing the interactions between long-chain unsaturated fatty acids and bacterial membranes. Importantly, this study underscores the potential of using biologically relevant model bacterial membrane systems to develop innovative strategies for combating bacterial infections and designing effective therapeutic agents.

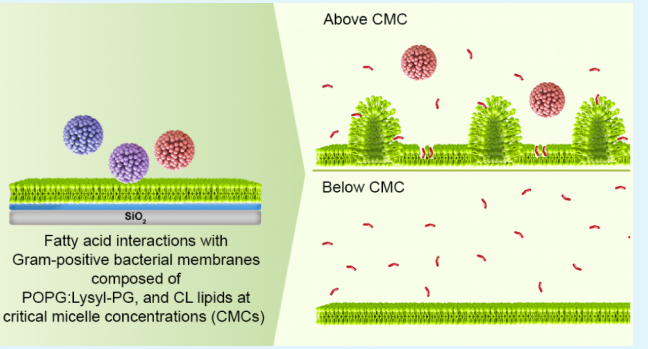

KEYWORDS: *antibacterial, antimicrobial, bacterial membranes, supported lipid bilayer, solvent-assisted lipid bilayer, fatty acids, critical micelle concentration*

INTRODUCTION

The bacterial lipid membrane, a vital structural component of bacterial cells, plays a pivotal role in various biological processes and has garnered significant attention in the fields of microbiology, drug development, and antimicrobial research.[1−5] This lipid bilayer membrane enveloping the bacterial cells not only acts as a protective barrier against external threats but also serves as a dynamic interface for crucial biomolecular interactions.[2,6−8] Therefore, understanding the intricate nature of these interactions is paramount for advancing our knowledge of bacterial resistance mechanisms, combating bacterial infections, and developing novel therapeutic agents, such as fatty acid-based drugs.[9,10] Furthermore, as the emergence of antibiotic-resistant bacterial strains has underscored the urgent need to develop new strategies to combat bacterial infections, the design of antibacterial agents relies heavily on comprehending how these molecules interact with the bacterial plasma membrane, given its extensive array of lipids and proteins that can be targeted without developing multidrug resistance.[11−14] This knowledge not only aids in the development of more effective treatments but also allows for the prediction and prevention of resistance mechanisms that bacteria may employ. However, the study of bacterial membrane interactions presents its own set of challenges. Traditional *in vitro* biological assay methods often fall short in

Received: July 5, 2024
Revised: September 27, 2024
Accepted: September 29, 2024
Published: October 10, 2024

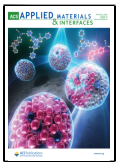

https://doi.org/10.1021/acsami.4c11158
ACS Appl. Mater. Interfaces 2024, 16, 56705−56717

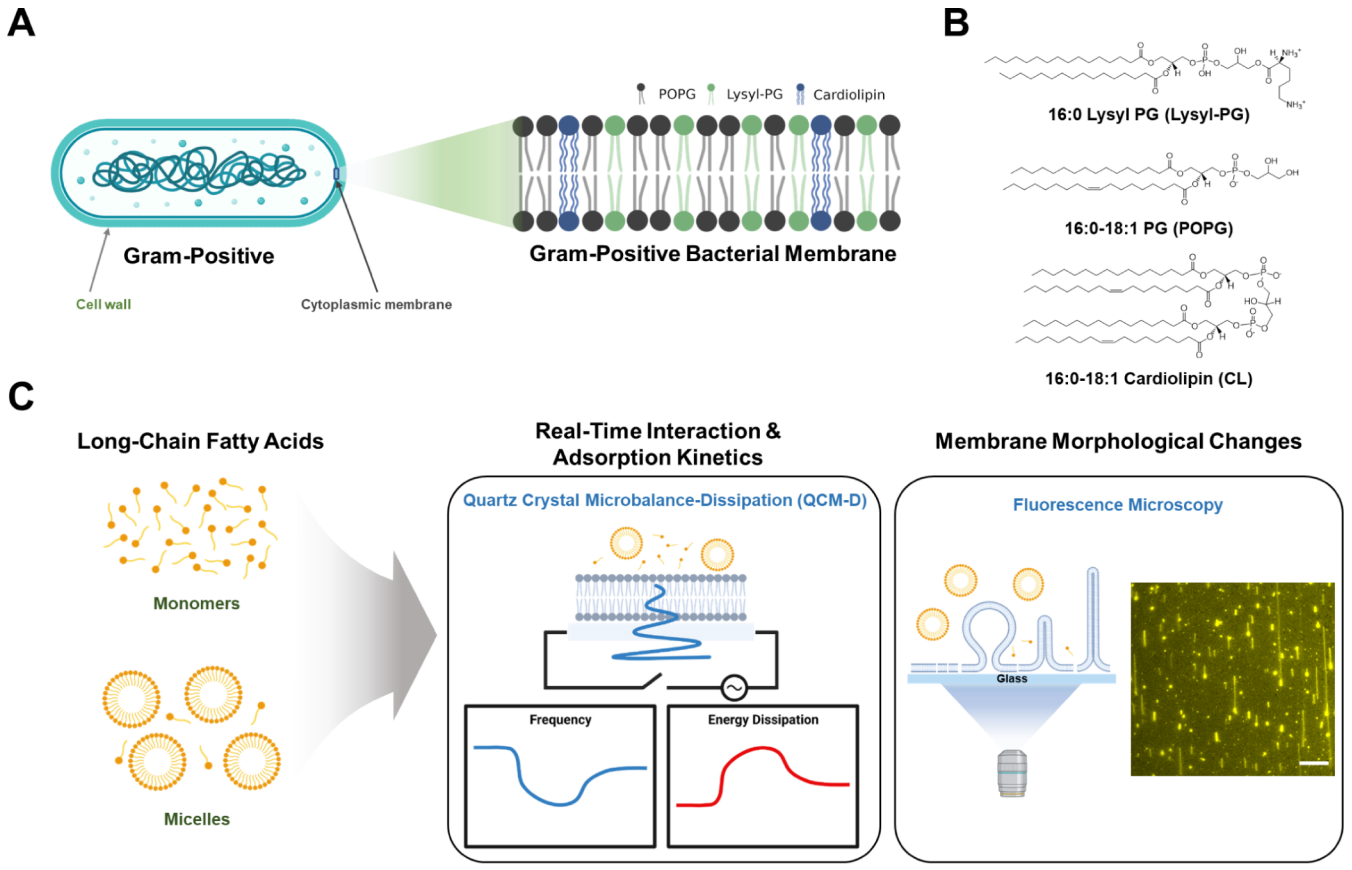

Figure 1. Experimental framework for investigating the interaction of antimicrobial long-chain fatty acids with model bacterial membrane platforms. (A) Schematics illustrating the membrane structure of Gram-positive bacteria with representative lipid compositions. (B) Chemical structure of the lipids utilized in model bacterial membrane platforms. Lysyl-PG is a bicationic membrane lipid, and POPG and CL are anionic membrane lipids present in the plasma membrane structure of Gram-positive bacteria. (C) Schematics illustrating the experimental strategy to characterize how long-chain fatty acids interact with model bacterial membranes through QCM-D and fluorescence microscopy.

accurately replicating the complex nature of bacterial membranes.[15,16] The presence of charged lipids, the nanometer dimensions, and other intricacies within bacterial membranes make it difficult to mimic their properties faithfully.[17] As a result, there is a pressing need for innovative approaches to investigate membrane interactions more accurately.

Supported lipid bilayers (SLBs) have great potential for advancing research in bacterial membranes as their planar geometry makes them compatible with a variety of surface sensing techniques and high-resolution imaging tools.[16] However, creating fluid and stable SLBs that faithfully mimic bacterial membranes, particularly those of complex compositions with a high percentage of charged lipids, remains challenging as the success of SLB formation by commonly used vesicle fusion relies on the preparation of high-quality vesicles and typically works within a limited range of material supports and lipid composition.[18] Specifically, bacterial membranes consist of intricate lipid mixtures that encompass anionic phospholipids such as cardiolipin (CL) and phosphatidylglycerol (PG), and cationic phospholipids like lysyl-PG.[17,19] The Gram-positive membrane contains around 80% charged lipids while the inner membrane of Gram-negative bacteria has around 30% charged lipids.[20,21] The presence of charged lipids results in robust electrostatic interactions between the lipids and the solid support surface, which, in turn, affects lipid motion within the model membrane.[22,23]

To overcome these challenges, we employed the solvent-assisted lipid bilayer (SALB) method to fabricate SLBs that mimic the characteristics of a Gram-positive bacterial membrane (Figure 1A,B). The SALB method represents an advanced and meticulously engineered approach that enables the precise fabrication of SLBs featuring various lipids including highly charged lipids, applied to a diverse range of substrates.[24,25] Upon successful fabrication of a model bacterial membrane, we then systematically investigated the real-time interactions between long-chain unsaturated fatty acids and the bacterial SLB platform (Figure 1C). Herein, our aim is to capture the physicochemical properties of the Gram-positive bacterial membranes, considering that long-chain fatty acids typically exhibit limited efficacy against Gram-negative bacteria.[26] The selection of long-chain unsaturated fatty acids was predicated on their potential as natural and effective entities with a low probability for developing resistance for developing novel antimicrobial agents (Figure S1).[27,28] Our previous research has focused on the molecular self-assembly and membrane interaction of these fatty acids with zwitterionic SLB platforms, providing valuable insights into their interactions with lipid bilayers.[29] Building upon this foundation, the scope of the SLB platforms is expanded to emulate bacterial membranes, thereby establishing a more biologically relevant model system. This account provides detailed insights into the molecular interactions of long-chain

https://doi.org/10.1021/acsami.4c11158
ACS Appl. Mater. Interfaces 2024, 16, 56705−56717

unsaturated fatty acids with Gram-positive bacterial membranes.

EXPERIMENTAL SECTION

Reagents. 1-Palmitoyl-2-oleoyl-*sn*-glycero-3-phospho-(1′-*rac*-glycerol) (POPG), 1,2-dipalmitoyl-*sn*-glycero-3-[phospho-rac-(3-lysyl(1-glycerol))] (Lysyl-PG), 1′,3′-bis[1-palmitoyl-2-oleoyl-*sn*-glycero-3-phospho]-glycerol (cardiolipin, CL), and 1,2-dioleoyl-*sn*-glycero-3-phosphoethanolamine-*N*-(lissamine rhodamine B sulfonyl) (ammonium salt) (Rh-PE) were obtained from Avanti Polar Lipids, Inc. (Alabaster, AL). Linolenic acid (LNA), linoleic acid (LLA), and oleic acid (OA) were purchased from Sigma-Aldrich (St. Louis, MO). Phosphate-buffered saline (PBS) buffer was purchased from Gibco (Carlsbad, CA). All solutions were prepared using Milli-Q-treated deionized water (>18 MΩ·cm) (Millipore, Billerica, MA).

Antimicrobial Fatty Acids Solution Preparation. To prepare stock solutions of LNA, LLA, and OA, precise quantities of each compound were dissolved in ethanol to a concentration of 50 mM. Aliquots of the stock solution were then diluted 100-fold using a PBS solution to obtain a final concentration of 500 μM. To enhance solubility, the test samples were heated to 70 °C for 30 min and subsequently cooled to room temperature. Further dilutions were performed in 2-fold increments. All solutions were freshly prepared immediately before each experiment.

Previous studies have demonstrated that the pK_a of the carboxyl group (~4.75) increases in a hydrophobic environment near physiological pH.[30] Moreover, the incorporation of long-chain fatty acids into zwitterionic liposomes imparts a negative charge on the liposome.[31,32] Therefore, the charge state of LNA and LLA is considered to be anionic in relation to the membrane, while OA is considered to be neutral with a protonated carboxylic acid moiety due to its high pK_a and its capacity to adjust the charge based on the solution's pH. This charge state information was used to elucidate the mechanistic interactions with model bacterial membranes.

Lipid Preparation for SLB Formation. Lipids for a Gram-positive mimetic model membrane composed of anionic POPG lipid, cationic Lysyl-PG lipid, and anionic CL lipid were mixed in a molar ratio of 65:30:5 in chloroform at a final concentration of 0.3 mg/mL. For fluorescence microscopy experiments, 0.5 mol % of Rh-PE, a negatively charged fluorescent DOPC analogue, was doped in SLBs. To prepare for SALB experiments, lipid films were initially dried using a stream of nitrogen gas and then stored under a vacuum overnight to remove the organic solvent, followed by dissolution in ethanol at 70 °C for 3 min to a concentration of 1 mg/mL. Before each experiment, the solution was further diluted in isopropanol.

Quartz Crystal Microbalance with Dissipation (QCM-D) Experiments. To investigate the formation of supported lipid bilayers (SLBs) and characterize the interaction between the antimicrobial fatty acids and the SLBs, QCM-D experiments were conducted using a four-channel Q-Sense E4 instrument (Q-Sense AB, Gothenburg, Sweden). The QCM-D technique tracks changes in the frequency (Δf) and energy dissipation (ΔD) of a piezoelectric quartz crystal sensor chip, which oscillates over time, and these changes provide insights into the mass and viscoelastic properties of the phospholipid film adsorbed on the surface of the chip. The sensor chips had a fundamental frequency of 5 MHz and were coated with a sputter-coated, 50 nm-thick layer of silicon dioxide (model no. QSX 303, Biolin Scientific). Before each experiment, the sensor chips were sequentially washed with 1% (w/v) SDS, water, and ethanol. Subsequently, they were dried with a gentle stream of nitrogen gas and treated with oxygen plasma for 1 min using an Expanded Plasma Cleaner (PDC-002, Harrick Plasma, Ithaca, NY). In the experiments, Gram-positive SLBs were initially formed using the solvent-assisted lipid bilayer (SALB) technique,[18] with heating at 70 °C. Each SLB was used only once per experiment. Initially, a baseline signal was recorded in an aqueous Tris buffer solution (10 mM Tris and 150 mM NaCl, pH 7.5). The solution was then replaced with an isopropanol solution, followed by the addition of 0.3 mg/mL Gram-positive mimetic membrane lipids in isopropanol solution, and finally the solvent was exchanged with a PBS solution to form the SLB. Once the lipid bilayer formation was complete, the test sample in PBS solution was added under continuous flow conditions, and a final washing step with PBS solution concluded the procedure. All liquid samples were introduced into the measurement chamber by using a peristaltic pump (Reglo Digital, Ismatec, Glattbrugg, Switzerland) under continuous flow conditions, with a flow rate of 50 μL/min. Throughout the experiments, the temperature in the measurement cell was maintained at room temperature (25.0 ± 0.5 °C). Measurement data were collected at the third (n = 3), fifth (n = 5), seventh (n = 7), and ninth (n = 9) overtones using the Q-Soft software program (Biolin Scientific). The presented data were obtained at the fifth overtone, and all data processing was carried out using the Q-Tools (Biolin Scientific) and OriginPro (OriginLab, Northampton, MA) software programs.

Time-Lapse Fluorescence Microscopy. Epifluorescence microscopy was used to observe membrane morphological changes in SLBs on silicon dioxide surfaces when treated with LNA, LLA, and OA. The experiments were performed using an Eclipse TI-E inverted microscope (Nikon, Tokyo, Japan) with a 60× magnification (NA = 1.49) oil-immersion objective lens (Nikon). Micrograph images were captured using an iXon 512 × 512 pixel EMCCD camera (Andor Technology, Belfast, Northern Ireland). The pixel size of the images was 0.267 × 0.267 μm^2. To illuminate the fluorescently labeled bacterial mimetic phospholipids (0.5 mol % Rh-PE), a fiber-coupled mercury lamp (Intensilight C-HGFIE, Nikon) was employed along with a TRITC filter. SLBs were fabricated on a glass coverslip as a substrate enclosed within a microfluidic flow-through chamber (sticky slide VI 0.4, Ibidi, Germany) via the SALB method.[18,30,31] Following SLB formation, the measurement chamber was rinsed with a PBS solution, after which the test compound was introduced under continuous flow conditions at a flow rate of 50 μL/min. To examine the time-dependence of the effect of the fatty acids on the SLBs, time-lapse micrographs were captured every 5 s for a total duration of 60 min at room temperature. The starting time, t = 0 s, was defined as the time at which the test solution was injected. The obtained images are presented with false-color visualizations, where yellow indicates lipid bilayer regions. The fractional surface area of membrane defects within SLBs was quantified and analyzed using the ImageJ software program (National Institutes of Health, Bethesda, MD, USA).

Fluorescence Recovery after Photobleaching (FRAP) Measurements. FRAP techniques were employed before and after treatment with the test compounds to measure the lateral diffusivity of the SLBs labeled with Rh-PE lipids. Photo-

https://doi.org/10.1021/acsami.4c11158
ACS Appl. Mater. Interfaces 2024, 16, 56705−56717

bleaching was achieved using a 532 nm, 100 mW laser (Klastech Laser Technologies, Dortmund, Germany) to create circular spots with diameters of 20 μm. The photobleaching process lasted 5 s, and fluorescence micrographs were captured every 2 s for a total of 120 s to monitor the fluorescence recovery. The lateral diffusion coefficients were derived from the FRAP data using a Hankel transform method[32] performed using Matlab (MathWorks, USA).

Time-Killing Kinetics Analysis. An overnight culture of *Staphylococcus aureus* MW2[33] was diluted 1:10,000 into 25 mL of tryptic soy broth (TSB) in a 250 mL Erlenmeyer flask. This diluted culture was incubated at 37 °C while being shaken at 200 rpm until the OD_{600} reached 0.05, indicating the exponential growth phase. The culture was then mixed with an equal volume of prewarmed TSB containing double the target concentrations of the compounds in the wells of a 96-well assay block (Bioneer cat# 90063, Daejeon, South Korea). The assay block was incubated at 37 °C with shaking at 450 rpm. Samples were taken hourly and serially diluted 10-fold in PBS. The diluted samples were plated on Mueller−Hinton (MH, BD cat# 275730) agar. Following overnight incubation at 37 °C, the number of colonies was counted to determine the number of viable cells. The experiment was independently repeated three times.

Membrane Permeability Assessment. The extent of MRSA membrane permeabilization by fatty acid compounds was assessed using the membrane-impermeable DNA-binding fluorescent dye SYTOX Green (ThermoFisher cat# S7020) based on a previously established procedure.[34] Briefly, *S. aureus* MW2 cells in the exponential growth phase were washed three times with PBS and adjusted to an OD_{600} of 0.4. Subsequently, SYTOX Green was added to the washed cell suspension at a final concentration of 5 μM. The cell suspension was then incubated in a dark chamber at room temperature for 30 min. Following this, a 50 μL aliquot from the SYTOX Green-bacterial cell mixture was dispensed into each well of a black, clear-bottom 96-well plate (Greiner Bio-One Cat. No. 665090), containing 50 μL of fatty acid compounds at concentrations ranging from 16 to 500 μM. Fluorescence measurements were conducted using a Cytation 5 multimode plate reader (BioTek, USA) at room temperature for 1 h, with excitation and emission wavelengths set at 485 and 525 nm, respectively. Experiments were performed in biological triplicates.

Evaluation of ATP Leakage in Bacterial Cells. The release of intracellular ATP from *S. aureus* MW2 cells was measured using the RealTime-Glo Extracellular ATP Assay (Promega, Madison, WI, USA), following the previously established procedure.[34] Exponential-phase *S. aureus* MW2 cells were adjusted to an OD_{600} of 0.4 after three washes with PBS. A mixture of ATP assay reagents was prepared at a 4× concentration according to the manufacturer's instructions. A black, clear bottom 96-well plate (Greiner Bio-One Cat. No. 665090) was used to prepare a series of test compound concentrations ranging from 16 to 500 μM, with each well containing 50 μL of the test compound and 50 μL of the bacterial cell suspension. The plates were statically incubated for 20 min at 37 °C. After incubation, a quadruple reagent mixture of 33.4 μL was added to each well, and luminescence was measured using a BioTek Cytation 5 multifunctional reader. All experiments were conducted in triplicate.

RESULTS AND DISCUSSION

Formation and Characterization of Model Bacterial Membranes. Bacteria are known to have limited capacity to modify their fundamental membrane lipid compositions compared to other targets, which contributes to a reduced likelihood of developing drug resistance.[35−37] It is therefore of great interest to study how antimicrobial agents interact with bacterial cell membranes to develop effective therapies based on their mechanisms of action. Many previous studies have utilized PG, PC, and PE as lipid compositions for model bacterial membranes. While such investigations have contributed to our understanding of membrane biophysics and the influence of individual lipid components on antimicrobial function, it is imperative to consider model membranes that closely replicate actual bacterial membranes. Therefore, we began by creating SLBs that closely mimic the plasma membranes of Gram-positive bacteria using the SALB method. The lipid compositions selected for the bacterial membranes matched those found in *S. aureus*. The Gram-positive bacterial SLBs were composed of POPG:Lysyl-PG:CL at the molar ratio of 65:30:5,[38] with anionic to cationic lipid proportions around 2:1,[39] at physiological pH. The significance of Lysyl-PG lipid lies in its ability to confer a positive charge to the cell envelope, creating a barrier against cationic compounds,[38] including antibiotics like daptomycin and host defense antimicrobial peptides (AMPs),[39] and the significance of CL lipid lies in its capability to resist mechanisms against membrane curvature-dependent AMPs, potentially rendering the bacteria susceptible to some of the novel antimicrobial agents.[40,41] Prior to implementing the SALB method, lipids with a high gel-to-liquid transition temperature (T_m) (*e.g.*, Lysyl-PG has a T_m of 40 °C and CL has a T_m of 62.5 °C[42,43] were mixed with ethanol at a temperature of 70 °C to enhance the solubility of the lipid mixture, thus enabling the reinstatement of fluidity within the SLBs. Tabaei et al. previously reported that isopropanol is the most effective organic solvent for depositing charged lipids onto a SiO_2 substrate using the SALB method.[18,24] Building upon this foundation, isopropyl alcohol was selected as the solvent medium to facilitate the solvent exchange step for the fabrication of model membranes, aligning with established protocols in the field.

To confirm the SLB formation, QCM-D experiments were conducted. The results indicated that the final resonance frequency (Δf) and energy dissipation (ΔD) shifts were −26.8 ± 1.1 Hz and 0.7 ± 0.4 × 10^{-6}, respectively, for Gram-positive bacterial SLB (Figure 2A), which were within the expected range for successful SLB formation.[44,45] To assess the structural integrity of the membranes, the lateral diffusion of fluorescently labeled Rh-PE lipids was monitored using FRAP analysis in Gram-positive bacterial SLB. The photobleached spots were near-completely recovered within 2 min with over 80% mobile fraction (Figure 2B), confirming the intact fluidity of the lipid bilayer membrane.[46] Moreover, the lateral diffusivity yielded a value of 0.47 ± 0.23 $\mu m^2\ s^{-1}$ (Figure S2B), indicating the slower lateral diffusion of Gram-positive bacterial membrane compared to a DOPC bilayer due to the presence of charged lipid species like Lysyl-PG and CL. The reduced lateral diffusion of Gram-positive bacterial SLB (Figure S2) can most likely be attributed to tighter lateral packing induced by the four-alkyl chain structure of CL.[47] This structural characteristic increases the average area per lipid molecule, impacting the mobility of the SLB. Moreover, the

https://doi.org/10.1021/acsami.4c11158
ACS Appl. Mater. Interfaces 2024, 16, 56705−56717

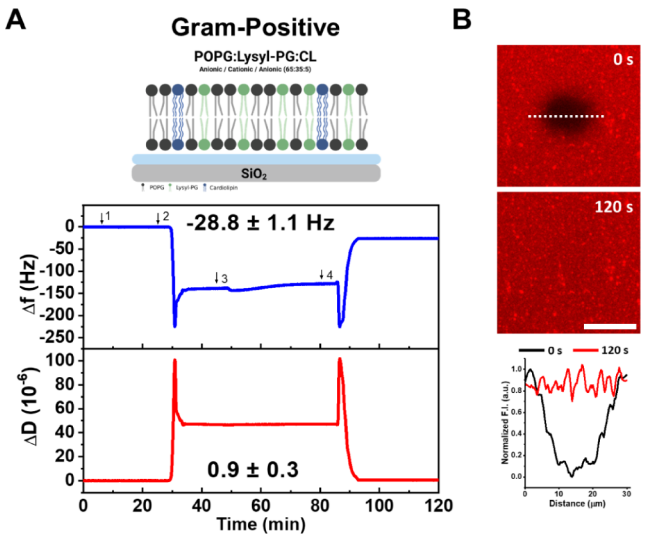

Figure 2. Formation of the model bacterial membrane using the SALB method on silicon dioxide via QCM-D and fluorescence microscopy. (A) QCM-D monitoring of the SALB method using lipid compositions for the Gram-positive bacterial membrane. Arrows indicate the injection of (1) buffer, (2) 2-propanol, (3) lipid mixture, and (4) buffer exchange. The final values of Δf and ΔD for the membrane are reported. All values are reported as the mean ± standard deviation from $n = 3$ measurements. (B) Fluorescence recovery after photobleaching (FRAP) analysis for the fluidity characterization of the Gram-positive membrane. Photobleaching was performed at $t = 0$ s, and the bleached spot corresponded to the dark spot in the center of the micrograph. The normalized fluorescence intensity (F.I.) as a function of distance across the bleached area (white dotted line in 0 s images) is presented in the corresponding cases. The F.I. was normalized by setting minimum and maximum F.I. values throughout the time as 0.0 and 1.0 au, respectively. The scale bar is 20 μm.

low mobility value is not significantly influenced by Lysyl-PG due to its structural similarity to PG, resulting in negligible electrostatic interactions with other phospholipids. Taken together, these findings demonstrate that Gram-positive biomimetic SLBs, composed of anionic and cationic phospholipids with high transition temperatures, can be successfully formulated using the SALB method in a near-physiological pH environment.

Mass and Viscoelastic Property Changes Induced by Antimicrobial Long-Chain Fatty Acids on Model Bacterial Membranes. We performed QCM-D experiments on the model bacterial membrane platforms to probe the interaction between model bacterial SLBs and antimicrobial long-chain unsaturated fatty acids. The QCM-D technique monitors alterations in frequency (Δf) and energy dissipation (ΔD) signals resulting from the dynamic interplay between model bacterial SLBs and antimicrobial fatty acids. These changes manifest as shifts in mass and modifications in viscoelastic characteristics. This study extends the previous research using single-component SLBs containing zwitterionic DOPC lipids[29] to model Gram-positive bacterial membrane SLBs. The aim was to enhance the understanding of membrane behaviors and mechanisms of action of potential antimicrobial long-chain fatty acids, particularly against Gram-positive bacteria, by targeting bacterial fatty acid synthesis and disrupting bacterial membranes.[26] Model Gram-positive bacterial SLBs were exposed to linolenic acid (LNA), linoleic acid (LLA), and oleic acid (OA) at fixed concentrations under continuous flow conditions, followed by a washing step with an equivalent buffer solution for 60 min. Real-time tracking of the temporal Δf and ΔD shifts with QCM-D measurements was carried out. Of note, $t = 0$ min denotes the bacterial SLB formation, and $t = 10$ min indicates the addition of fatty acids in the measurement chamber. The time-dependent binding and interaction kinetics observed for long-chain fatty acids are presented below.

Linolenic Acid (LNA) on Gram-Positive Bacterial SLBs. Figure 3 presents the effects of LNA on the interaction dynamics of model bacterial SLBs. When 500 μM LNA was applied to Gram-positive SLBs, there was a rapid decrease in both Δf to approximately -63.8 ± 0.8 Hz and ΔD to $12.8 \pm 0.5 \times 10^{-6}$ (Figure 3A). For the zwitterionic membranes, the maximum binding amount was approximately -39.2 ± 1.8 Hz and $8.6 \pm 0.2 \times 10^{-6}$.[29] With the charged membranes, the binding substantially increased, which may suggest that LNA attached to the charged membrane together with a large amount of solvent through stronger electrostatic attraction, leading to considerable membrane remodeling. Upon reaching the critical point, measurement responses began to reverse, with a swift rise in Δf and a decline in ΔD, ultimately stabilizing at -29.6 ± 2.1 Hz and $23.8 \pm 1.6 \times 10^{-6}$, respectively. Subsequent buffer washing led to partial membrane removal with a change in Δf to around -17.0 ± 0.6 Hz and ΔD to $6.2 \pm 0.2 \times 10^{-6}$, resulting in a net Δf increase of 10.1 ± 1.4 Hz and a net ΔD increase of $5.4 \pm 0.7 \times 10^{-6}$. Similarly, LNA exhibited a comparable attachment-detachment pattern on the Gram-positive membrane at 250 μM (Figure S5). The Δf signal decreased to -58.2 ± 1.9 Hz, increased after the critical point, and stabilized at -16.6 ± 2.1 Hz after buffer washing. The ΔD signal concomitantly increased to $15.5 \pm 0.7 \times 10^{-6}$ before stabilizing at $5.3 \pm 0.5 \times 10^{-6}$ after buffer washing.

Figure 3B illustrates a three-stage Δf *vs* ΔD plot after the LNA treatment. In the first stage, there is an increase in mass and a decrease in rigidity, indicating rapid incorporation of LNA into the membrane and subsequent membrane rearrangement between phospholipids and LNA molecules.[48] In the second stage, a decrease in mass and a further decrease in rigidity are observed, possibly suggesting an ongoing rearrangement and expulsion of entrapped solvent or material removal. Moreover, the lower harmonics exhibit higher frequency values, suggesting that the top layer is denser, possibly due to additional LNA molecules or the displacement of more phospholipids from the bottom layer in exchange for LNA. This is promptly succeeded by a slight decrease in mass and an increase in rigidity, implying the near-completion of membrane rearrangement and the commencement of phospholipid removal. During this stage, the shift from a relatively small spreading to the overlap of the third to ninth harmonics is evident upon buffer washing (Figure S4A), which indicates that the membrane removal affects both the bottom and top SLB layers similarly. Stage three involves a significant decrease in mass and an increase in rigidity upon buffer washing, signifying the removal of weakly interacting LNA attached to the phospholipids and a portion of the membrane. LNA, with the highest number of double bonds and the lowest pK_a, is more likely to be deprotonated, reducing hydrophobic interaction energy and promoting the movement of the anionic form of fatty acid toward the aqueous phase due to

https://doi.org/10.1021/acsami.4c11158
ACS Appl. Mater. Interfaces 2024, 16, 56705−56717

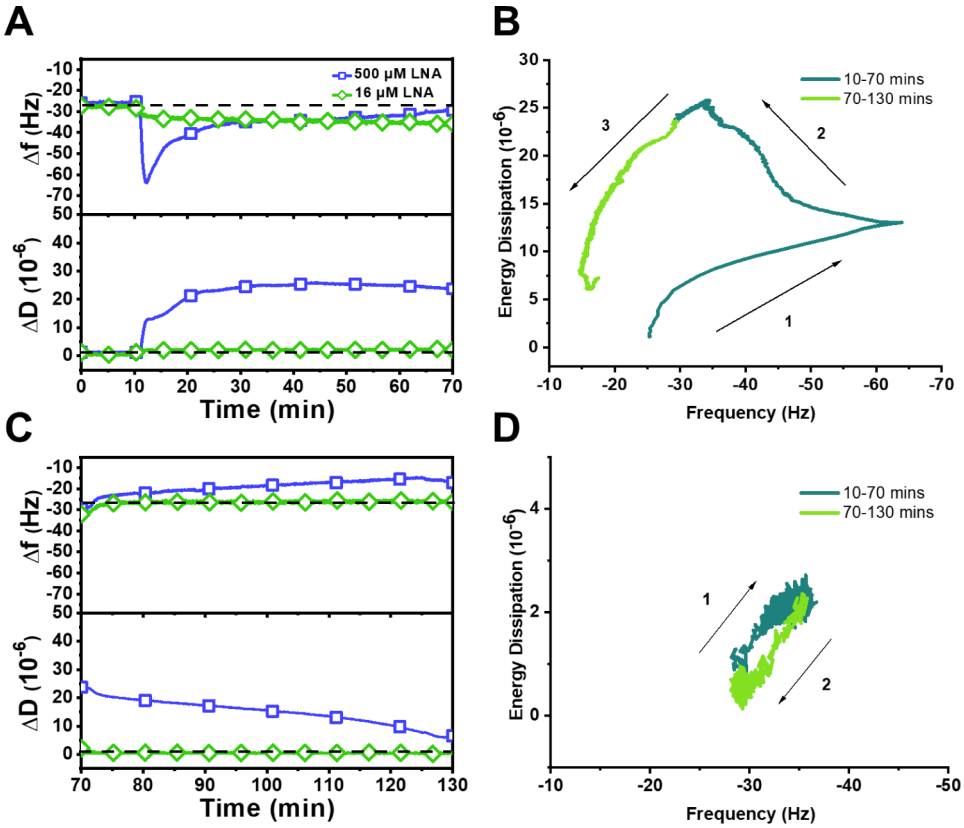

Figure 3. QCM-D investigation of LNA treatments on model bacterial membranes at pH 7.5. (A,C) Representative Δf and ΔD *vs* time plots of LNA-treated Gram-positive bacterial membranes at concentrations of 500 μM (above CMC) and 16 μM (below CMC), and (B,D) their respective Δf and ΔD plots. Fatty acid was added at t = 10 min, followed by a buffer washing at t = 70 min. The dotted line in panels (A,C) represents the typical measurement responses for SLB formation.

the formation of hydrogen bonds with the water molecules,[49] resulting in weak interaction with the membrane.

By contrast, at concentrations below CMC (160 μM), LNA exhibited slow attachment to the Gram-positive membrane (Figures 3C and S5), followed by rapid detachment without inducing a discernible ΔD shift, indicating the integrity of the rigid membrane without membrane remodeling. Figure 3D shows a two-stage Δf *vs* ΔD plot after LNA treatment at low concentration. Stage one shows a moderate increase in mass and decrease in rigidity, directly followed by a decrease in mass and an increase in rigidity, indicating negligible interaction between LNA and the membrane.

Linoleic Acid (LLA) on Gram-Positive Bacterial SLBs. Figure 4 presents the mass and viscoelastic changes of model bacterial SLBs as functions of LLA concentration. Treatment with 500 μM LLA led to a rapid reduction in Δf to -59.0 ± 3.0 Hz and a corresponding increase in ΔD to $17.4 \pm 2.3 \times 10^{-6}$ on Gram-positive SLBs (Figure 4A). Following the washing step, the Δf and ΔD signals gradually stabilized at around -18.7 ± 2.8 Hz and $26.8 \pm 3.4 \times 10^{-6}$, respectively, resulting in a net Δf increase of 9.1 ± 1.0 Hz and a net ΔD increase of $26.7 \pm 3.6 \times 10^{-6}$. This observed trend was consistent across varying LLA concentrations, including 250, 125, and 62.5 μM (Figure S6), albeit at a slower rate than LNA. The lowest harmonics detected the largest addition of mass and decrease in rigidity, suggesting that LLA is mainly attached to the upper part of the SLB layer (Figure S4B). Interestingly, the higher harmonics corresponding to the bottom layer detected the largest mass decrease, possibly indicating that the phospholipid species could be removed primarily from the bottom layer in exchange for LLA.

In Figure 4B, the Δf *vs* ΔD plot illustrates a three-stage process following 500 μM LLA treatment. Similar to LNA, stage one showed an increase in mass and a decrease in rigidity, indicating incorporation of LLA into the membrane, albeit at a slower rate. After reaching the turning point, stage two involved a concomitant decrease in both mass and rigidity, indicating membrane rearrangement. In the final stage, there was a decrease in mass and an increase in rigidity. Notably, the net mass change was smaller in magnitude, and the net dissipation change was almost negligible with evident increased harmonic spreading after buffer washing (Figure S4B). This behavior indicates that the enhanced incorporation of LLA resulted in a more fluidic SLB, leading to reduced membrane removal.

Conversely, at concentrations below CMC (60 μM), LLA monomers had a negligible effect on the Gram-positive membrane. However, the longer trend line of LLA with higher frequency and dissipation responses signifies that LLA had more impact on the membrane even at concentrations below CMC due to its physicochemical property differences (Figure 4D).

Oleic Acid (OA) on Gram-Positive Bacterial SLBs. Figure 5 illustrates the impact of OA on the changes in Δf and ΔD signals within model bacterial membranes. Treatment with 500 μM OA led to a reduction in the Δf signal to -68.5 ± 6.0 Hz and an increase in the ΔD signal to $18.5 \pm 1.8 \times 10^{-6}$ (Figure 5A). After buffer washing, the Δf and ΔD signals stabilized at

https://doi.org/10.1021/acsami.4c11158
ACS Appl. Mater. Interfaces 2024, 16, 56705−56717

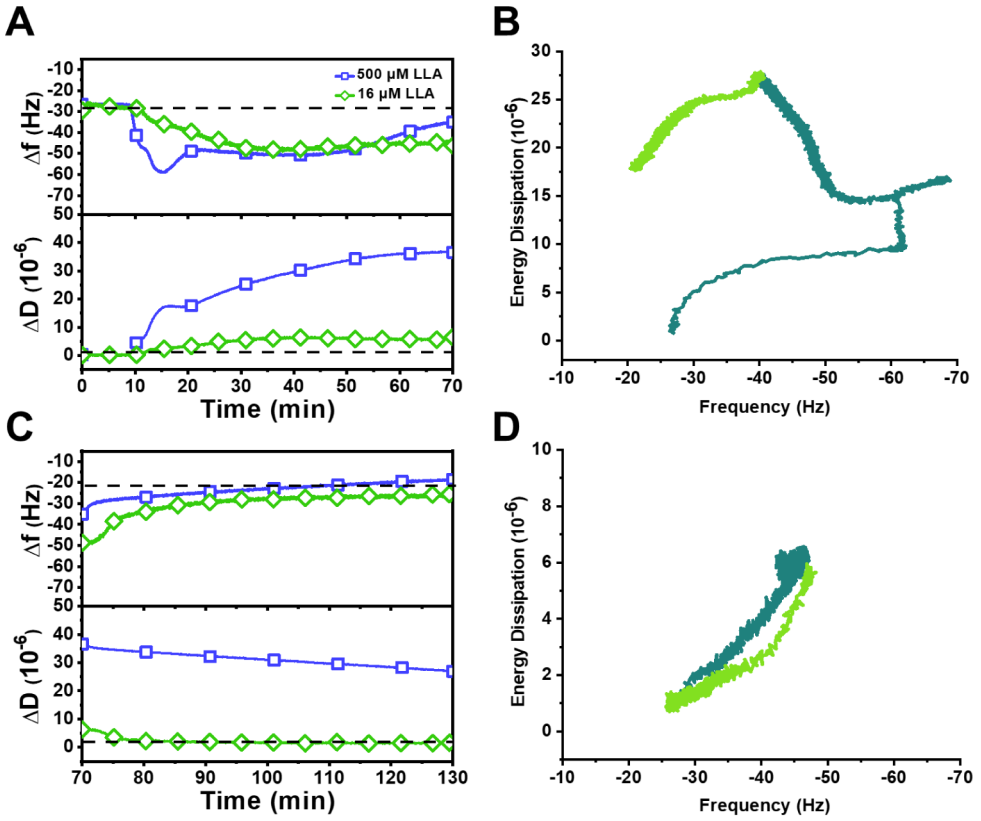

Figure 4. QCM-D investigation of LLA treatments on model bacterial membranes at pH 7.5. (A,C) Representative Δf and ΔD *vs* time plots of LLA-treated Gram-positive bacterial membranes at concentrations of 500 μM (above CMC) and 16 μM (below CMC), and (B,D) their respective Δf and ΔD plots. Fatty acid was added at t = 10 min, followed by a buffer washing at t = 70 min. The dotted line in panels (A,C) represents the typical measurement responses for SLB formation.

around -38.5 ± 4.3 Hz and $22.1 \pm 1.7 \times 10^{-6}$, respectively, resulting in a net Δf decrease of 11.3 ± 0.9 Hz and a net ΔD increase of $21.4 \pm 0.5 \times 10^{-6}$. Among the three tested agents, OA induced the most substantial changes in the physicochemical properties of the Gram-positive bacterial SLBs. The significant harmonic spreading observed with OA treatment indicates notable changes in dissipation, suggesting the formation of a softer and thicker SLB. This effect was observed on both the top and bottom layers of the membrane.

Figure 5B depicts the three distinctive stages for the OA-treated SLB. In the initial stage, treatment with 500 μM OA resulted in an increase in mass and a decrease in rigidity. Upon reaching the inflection point, there was a loss in mass followed by an increase in mass, whereas the rigidity continuously decreased (stage two). This may indicate molecule rearrangement, leading to the formation of a thicker and more fluidic membrane. This interpretation is supported by the dramatic harmonic spreading in Figure S4C. After buffer washing, stage three involved a decrease in mass with negligible viscoelastic property change, potentially indicating the incorporation of the protonated form of OA into the bilayer membrane to reach energetic minimum.[49] Previous reports suggest that the protonated carboxylic acid moiety enables deeper lipid bilayer penetration and plays a crucial role in membrane disruption.[50]

Interestingly, at concentrations below the CMC (20 μM), OA displayed gradual attachment to Gram-positive membranes with minimal changes in dissipation, even after buffer washing (Figure 5C). This phenomenon may be attributed to the ability of OA to self-aggregate into vesicles even at concentrations below CMC,[51] allowing it to attach to the membrane even at low concentrations. As evidenced by the uniform spreading of the harmonics in Figure S4E, OA produced similar effects on both sides of the SLB, indicating its influence on the entire bilayer structure.

Observation of Membrane Morphological Responses in Model Bacterial Membranes. We employed time-lapse fluorescence microscopy to directly observe the morphological changes in Gram-positive bacterial SLBs induced by antimicrobial long-chain fatty acids (Figure 6). Following the establishment of the bacterial biomimetic SLB, long-chain fatty acids were introduced under continuous flow conditions. The time point at which the fatty acid solution reached the measurement chamber was designated as t = 0 min. The concentrations of the fatty acids used in this study were determined based on their CMC values measured by fluorescence spectroscopy.[29,52,53] Specifically, the concentrations selected were as follows: 500 and 63 μM for LNA, 250 and 31 μM for LLA, and 125 and 16 μM for OA. The results obtained for these compounds are presented below.

Treatment with 500 μM LNA, above its CMC, induced the rapid formation of static nucleation sites with bright spots on the Gram-positive SLB. These sites developed into short tubules that remained stable over time and persisted on the membrane even after buffer washing, resulting in a total spot area of 1489.0 ± 104.7 μm^2 (Figure 6A). Notably, the size of the short tubules and aggregates was small, and there was a reduction in the fluorescence intensity of the background. This observation potentially indicates a weak interaction between the LNA and the membrane and suggests signs of membrane removal after buffer washing, as observed in QCM-D

https://doi.org/10.1021/acsami.4c11158
ACS Appl. Mater. Interfaces 2024, 16, 56705−56717

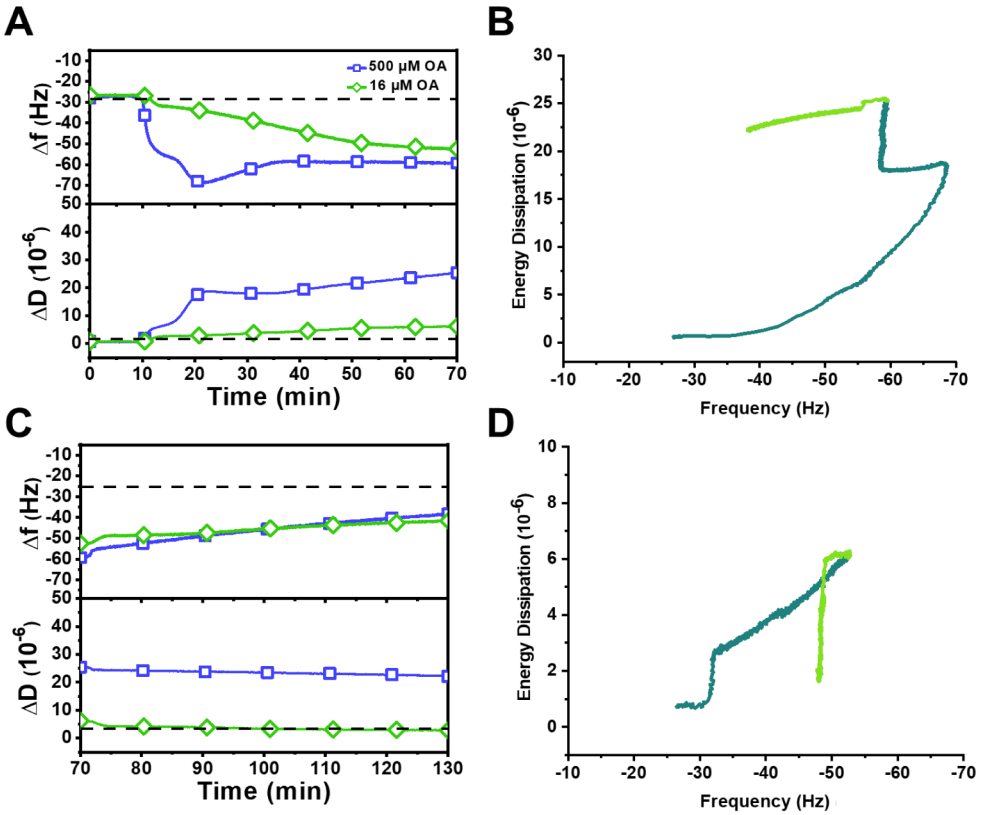

Figure 5. QCM-D investigation of OA treatments on model bacterial membranes at pH 7.5. (A,C) Representative Δf and ΔD *vs* time plots of OA-treated Gram-positive bacterial membranes at concentrations of 500 μM (above CMC) and 16 μM (below CMC), and (B,D) their respective Δf and ΔD plots. Fatty acid was added at t = 10 min, followed by buffer washing at t = 70 min. The dotted lines in panels (A,C) represent the typical measurement responses for SLB formation.

experiments. In contrast, 63 μM LNA, below its CMC, led to minimal morphological changes, with only a few short tubules observed on the SLB surface, covering a total area of 2.2 ± 0.4 μm^2. This indicates minimal morphological changes on the SLB membrane at concentrations below the CMC (Figure S8A).

Upon exposure to 250 μM LLA, a dense array of bright spots protruded from the membrane, remaining relatively unchanged for 60 min. Following the buffer washing step, these bright spots became notably more pronounced, covering an area of 2158.0 ± 77.8 μm^2. Compared with LNA, the aggregates formed by LLA were visibly larger, with areas of higher fluorescence intensity in the background after buffer washing. This observation is consistent with the smaller net mass change and the detection of the highest mass decrease in the higher harmonics, resulting in the removal of the bottom layer in exchange for LLA molecules (Figure S4B). When exposed to 31 μM LLA, there were marginal morphological changes on the membrane, indicated by few discernible spots. LLA exhibited CMC-dependent membrane remodeling and removal on the Gram-positive membrane. This trend is closely aligned with the interaction kinetics of LNA with the Gram-positive membrane, as observed through QCM-D signal responses, which revealed that the attachment and detachment kinetics of fatty acids are observed at concentrations above the CMC, accompanied by significant changes in energy dissipation. Notably, the membrane underwent less property changes with LLA than with LNA, likely due to LLA's straighter hydrophobic tail, which confers a stronger insertion capacity.[49]

Similar morphological responses and attachment phenomena were observed on the membrane throughout the 60 min when treated with 125 μM OA, resulting in the highest spot area of 2434.9 ± 125.7 μm^2. Notably, the fluorescence intensity of the background remained relatively unchanged throughout the treatment and the washing steps, consistent with the conclusions of the QCM-D fingerprinting analysis. OA displayed membrane attachment and remodeling patterns similar to those observed with LNA and LLA, but without membrane removal and with deeper insertion into the bilayer membrane, as indicated by smaller aggregates. At a concentration of 16 μM, OA instigated the formation of conspicuous spot protrusions on the membrane surface, and these protrusions remained unaffected even after the buffer washing step, providing evidence of OA's insertion into the membrane. Notably, the number of persistent bright spots (781.5 ± 51.4 μm^2) surpassed those observed with LNA and LLA treatments at concentrations below CMC, underscoring the CMC-independent activity profile of OA. This phenomenon may be attributed to OA having the highest pK_a value among the three fatty acids, thereby increasing the probability of the fatty acid being protonated.[49] This results in a higher electrostatic interaction force between OA and anionic phospholipids within the bacterial membrane, potentially pulling a larger fraction of OA deep into the lipid bilayer. Consequently, OA can interact with the Gram-positive membrane at concentrations above and below its respective CMC value. Notably, OA exhibited membrane activity even at concentrations below CMC, suggesting robust adhesion, likely attributed to its efficient integration into CL lipids.[54]

https://doi.org/10.1021/acsami.4c11158
ACS Appl. Mater. Interfaces 2024, 16, 56705−56717

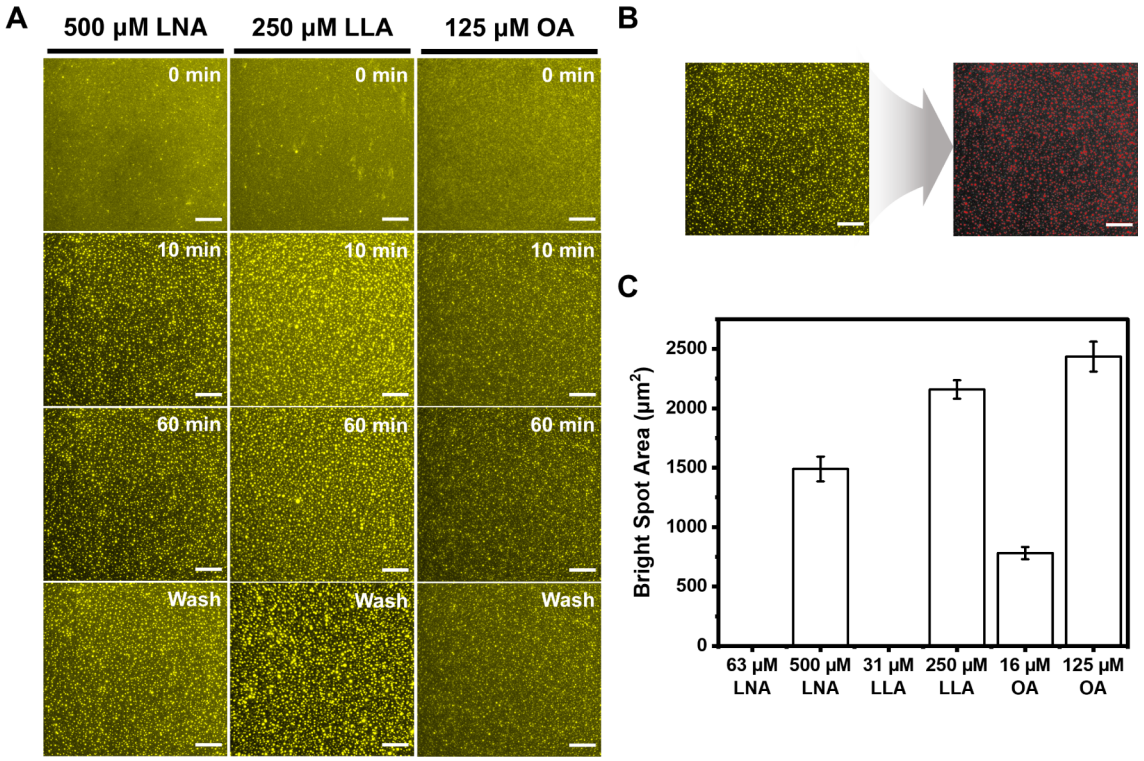

Figure 6. Time-lapse microscopic observation of membrane morphological responses in model bacterial membranes triggered by fatty acid treatments at concentrations below and above the CMC. (A) Representative sequential image snapshots depicting the morphological change of Gram-positive bacterial membrane under LNA treatment at 500 μM. (B) Representative analysis for calculating spot area formed on SLBs. (C) Total area of spot formation on SLBs after buffer washing. Data are reported as the mean ± standard deviation from n = 3 measurements. The scale bar is 20 μm.

Antimicrobial Potency of the Membrane-Active Long-Chain Unsaturated Fatty Acids on *S. aureus* MW2. Due to issues related to the solubility of fatty acids, MIC measurements were not possible in our study. Instead, we concentrated on assessing the compounds' bactericidal properties. The observed bactericidal effects against *S. aureus* MW2 generally corresponded with the behaviors observed in our model of Gram-positive membranes, highlighting the significance of our model bacterial membrane systems in comprehending antimicrobial activities.

To characterize the antimicrobial activity of LNA, LLA, and OA, we evaluated the bactericidal activity of the fatty acids against *S. aureus* MW2 within the concentration range of 16–500 μM (Figure 7A). Treatment with LNA for 4 h led to approximately a 4-log reduction in bacterial viability at concentrations equal to or more than 125 μM. While 4 h treatment with LLA resulted in approximately a 4-log reduction in bacterial viability at concentrations equal to or more than 250 μM, treatment with OA for the same time frame caused about a 3-log decrease in *S. aureus* MW2 viability at 500 μM. The concentrations at which the three fatty acid compounds induced more than 3-log killing are consistent with the concentrations at which those compounds interacted with the model bacterial membranes (Figures S5–S7). These findings indicate that LNA, LLA, and OA exhibit antimicrobial activity against *S. aureus* MW2 within concentration ranges that align with their biophysical interactions with model bacterial membranes. Notably, the observed bactericidal activity of OA is not directly proportional to the biophysics data. One possible rationale for this phenomenon is that not all neutral OA molecules exhibit membrane activity due to their tendency to self-aggregate at physiological pH, forming self-assembled complexes or dimers that may lack or have reduced antimicrobial efficacy against bacteria.[55] This phenomenon may also be attributed to the CMC-independent behavior exhibited by OA. In addition, a complex sequence of biological events transpires between the action of an antimicrobial agent on its primary target and the eventual demise of the bacteria. Several studies have illustrated that the disruption of the primary target by an antibiotic initiates subsequent biological processes, such as the accumulation of reactive oxygen species (ROSs),[56] alterations in metabolisms,[57] or impairment of cellular components,[58] which collectively lead to bacterial cell death.[59]

To complement this study, we further evaluated the membrane-active abilities of LNA, LLA, and OA by conducting membrane permeability and cellular ATP leakage assays (Figure 7B,C). LNA resulted in a rapid increase in SYTOX Green fluorescence at concentrations between 125 and 500 μM, LLA at concentrations between 63 and 500 μM, and OA at concentrations between 31 and 500 μM. Membrane disrupting antimicrobial compounds can cause leakage of intracellular ATP.[34,55] To ascertain whether the fatty acid treatment results in ATP leakage from inside the bacterial cells, we employed the ATP luminescence assay. A significant increase in luminescence was observed in *S. aureus* MW2 cells treated with LNA at concentrations between 125and 500 μM, LLA at concentrations between 63 and 500 μM, and OA at concentrations between 31and 500 μM. Overall, the results indicate that the test compounds induce membrane disruption in the bacteria in a CMC-dependent manner.[29]

https://doi.org/10.1021/acsami.4c11158
ACS Appl. Mater. Interfaces 2024, 16, 56705–56717

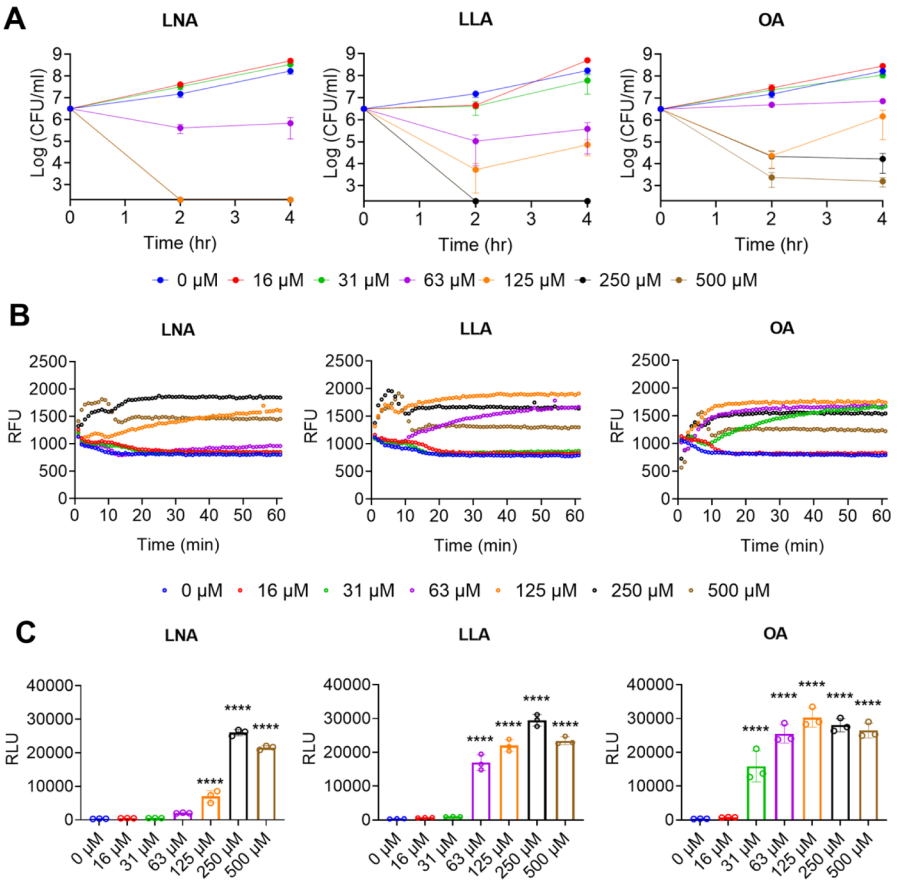

Figure 7. LNA, LLA, and OA penetrate the cell membrane bilayers of *S. aureus* MW2, demonstrating antimicrobial activity. (A) Exponential-phase *S. aureus* MW2 cells were treated with concentrations ranging from 16 to 500 μM for 4 h. CFU (colony forming units) counts of surviving cells were determined by serial dilution and plating on MH agar plates every 2 h. Results are shown as mean ± standard deviation (n = 3). Data points on the x-axis are below the detection limit (2×10^2 CFU/mL). (B) After treatment of *S. aureus* MW2 with LNA, LLA, and OA for 60 min, membrane permeabilization was estimated using SYTOX Green (Ex 485 nm and Em 525 nm). Results represent the mean of three independent experiments. (C) Leakage of intracellular ATP from *S. aureus* MW2 cells treated with LNA, LLA, and OA for 20 min was monitored by using an ATP luminescence assay. Individual data points are shown, and error bars represent mean ± SD (n = 3). Statistical differences were analyzed using one-way ANOVA followed by Tukey's multiple comparisons test (****$p < 0.0001$).

Overall, it is noteworthy that the interaction dynamics of long-chain fatty acids on Gram-positive bacterial membranes is relatively in line with the bactericidal efficacy against *S. aureus* MW2. The results of the membrane permeabilization and ATP leakage assay results corresponded closely to their individual CMC values, indicating a CMC-dependent interaction behavior on Gram-positive bacterial membranes. Conversely, OA exhibited bactericidal effects at a concentration exceeding its CMC value, suggesting a CMC-independent interaction with Gram-positive bacterial membranes. This correlation underscores the importance of utilizing biologically relevant model systems of bacterial membranes in antimicrobial studies.

CONCLUSIONS

In conclusion, our study explored the intricate interactions between antimicrobial long-chain fatty acids (LNA, LLA, and OA) and Gram-positive bacterial membranes using model bacterial lipid bilayers fabricated via the solvent-assisted lipid bilayer (SALB) method. Through a combination of QCM-D measurement and fluorescence microscopy imaging, we elucidated that LNA and LLA exhibit CMC-dependent interactions with Gram-positive membranes, leading to significant membrane remodeling and removal at concentrations exceeding their respective CMC values. In contrast, OA demonstrated a CMC-independent activity characterized by penetration into the membrane across all concentrations tested. The observed bactericidal effects against *S. aureus* MW2 generally aligned with the behaviors observed on the model Gram-positive membrane, reinforcing the relevance of our model bacterial membrane systems in understanding antimicrobial activities. These findings provide valuable insights into the diverse mechanisms by which long-chain unsaturated fatty acids exert their effects on Gram-positive bacterial membranes. Moreover, they underscore the importance of utilizing biologically relevant model systems to advance our understanding of antimicrobial mechanisms and contribute to the development of effective antibacterial treatments. Furthermore, the potential of long-chain fatty acids in combating antibiotic-resistant strains is highlighted. Nevertheless, further investigations are warranted to evaluate their *in vivo* efficacy and potential cytotoxicity, ensuring their safety and efficacy for clinical applications.

ASSOCIATED CONTENT

Supporting Information

The Supporting Information is available free of charge at https://pubs.acs.org/doi/10.1021/acsami.4c11158.

https://doi.org/10.1021/acsami.4c11158
ACS Appl. Mater. Interfaces 2024, 16, 56705−56717

Molecular structure for antimicrobial long-chain fatty acids used in this study, FRAP analysis for the mobility characterization of Gram-positive bacterial SLBs, QCM-D traces for Gram-positive bacterial SLB formations, QCM-D investigation of LNA, LLA, and OA treatments on model bacterial membranes at concentrations above and below CMC values at different harmonics, QCM-D investigation of concentration-dependent LNA treatments on model Gram-positive bacterial membranes as functions of time of 16, 31, 250, and 500 μM until 70 min, QCM-D investigation of concentration-dependent LLA treatments on model Gram-positive bacterial membranes as functions of time of 16, 31, 250, and 500 μM until 70 min, QCM-D investigation of concentration-dependent OA treatments on model Gram-positive bacterial membranes as functions of time of 16, 31, 250, and 500 μM until 70 min, and time-lapse microscopic observation of membrane morphological responses in model Gram-positive bacterial membranes triggered by LNA, LLA, and OA at concentrations below CMC (PDF)

AUTHOR INFORMATION

Corresponding Author

Nam-Joon Cho − *School of Materials Science and Engineering, Nanyang Technological University, Singapore 639798, Singapore; Singapore-HUJ Alliance for Research and Enterprise, Singapore HUJ Alliance Research Enterprise (SHARE) 1 CREATE Way, Singapore 138602, Singapore;* orcid.org/0000-0002-8692-8955; Email: njcho@ntu.edu.sg

Authors

Sungmin Shin − *School of Materials Science and Engineering, Nanyang Technological University, Singapore 639798, Singapore; Singapore-HUJ Alliance for Research and Enterprise, Singapore HUJ Alliance Research Enterprise (SHARE) 1 CREATE Way, Singapore 138602, Singapore*

Jingyeong Yu − *College of Pharmacy, Graduate School of Pharmaceutical Sciences, Ewha Womans University, Seoul 03760, Republic of Korea*

Hyunhyuk Tae − *School of Materials Science and Engineering, Nanyang Technological University, Singapore 639798, Singapore;* orcid.org/0000-0002-0459-5879

Yilin Zhao − *School of Chemistry, Chemical Engineering and Biotechnology, Nanyang Technological University, Singapore 637459, Singapore*

Dongping Jiang − *School of Materials Science and Engineering, Nanyang Technological University, Singapore 639798, Singapore*

Yuan Qiao − *School of Chemistry, Chemical Engineering and Biotechnology, Nanyang Technological University, Singapore 637459, Singapore;* orcid.org/0000-0003-0188-0700

Wooseong Kim − *College of Pharmacy, Graduate School of Pharmaceutical Sciences, Ewha Womans University, Seoul 03760, Republic of Korea*

Complete contact information is available at: https://pubs.acs.org/10.1021/acsami.4c11158

Notes

The authors declare no competing financial interest.

ACKNOWLEDGMENTS

The authors thank Dr. Bo Kyeong Yoon and Dr. Joshua A. Jackman for their valuable discussions. This work was supported by the National Research Foundation of Korea (NRF) grants funded by the Ministry of Science and ICT (2021K1A4A7A0209781012) and by the National Institute of Health (NIH) grants funded by the Korea Disease Control and Prevention Agency (KDCA) (2022ER240600). This work was also supported by the National Research Foundation, Singapore, under its Campus for Research Excellence and Technological Enterprise (CREATE) program and the Ministry of Education (MOE) in Singapore under grants RG111/20 and RG34/22. In addition, this research was supported by the Procter & Gamble Company (P&G) under grants APG2013/129 and H23PG10011.

REFERENCES

(1) MacDermott-Opeskin, H. I.; Gupta, V.; O'Mara, M. L. Lipid-mediated antimicrobial resistance: a phantom menace or a new hope? *Biophys. Rev.* **2022**, *14* (1), 145−162.

(2) Li, S.; Ren, R.; Lyu, L.; Song, J.; Wang, Y.; Lin, T.-W.; Brun, A. L.; Hsu, H.-Y.; Shen, H.-H. Solid and Liquid Surface-Supported Bacterial Membrane Mimetics as a Platform for the Functional and Structural Studies of Antimicrobials. *Membranes* **2022**, *12* (10), 906.

(3) Ganesan, N.; Mishra, B.; Felix, L.; Mylonakis, E. Antimicrobial Peptides and Small Molecules Targeting the Cell Membrane of Staphylococcus aureus. *Microbiol. Mol. Biol. Rev.* **2023**, *87* (2), No. e00037.

(4) Fjell, C. D.; Hiss, J. A.; Hancock, R. E. W.; Schneider, G. Designing antimicrobial peptides: form follows function. *Nat. Rev. Drug Discovery* **2012**, *11* (1), 37−51.

(5) Desbois, A. P.; Smith, V. J. Antibacterial free fatty acids: activities, mechanisms of action and biotechnological potential. *Appl. Microbiol. Biotechnol.* **2010**, *85* (6), 1629−1642.

(6) Sarkis, J.; Vié, V. Biomimetic Models to Investigate Membrane Biophysics Affecting Lipid−Protein Interaction. *Front. Bioeng. Biotechnol.* **2020**, *8*, 270.

(7) Lombard, J. Once upon a time the cell membranes: 175 years of cell boundary research. *Biol. Direct* **2014**, *9* (1), 32.

(8) Ramos-Martín, F.; D'Amelio, N. Biomembrane lipids: When physics and chemistry join to shape biological activity. *Biochimie* **2022**, *203*, 118−138.

(9) Yoon, B. K.; Jackman, J. A.; Kim, M. C.; Sut, T. N.; Cho, N.-J. Correlating Membrane Morphological Responses with Micellar Aggregation Behavior of Capric Acid and Monocaprin. *Langmuir* **2017**, *33* (11), 2750−2759.

(10) Yoon, B. K.; Jackman, J. A.; Kim, M. C.; Cho, N.-J. Spectrum of Membrane Morphological Responses to Antibacterial Fatty Acids and Related Surfactants. *Langmuir* **2015**, *31* (37), 10223−10232.

(11) Frieri, M.; Kumar, K.; Boutin, A. Antibiotic resistance. *J. Infect. Public Health* **2017**, *10* (4), 369−378.

(12) Chellat, M. F.; Raguž, L.; Riedl, R. Targeting antibiotic resistance. *Angew. Chem., Int. Ed.* **2016**, *55* (23), 6600−6626.

(13) Silhavy, T. J.; Kahne, D.; Walker, S. The bacterial cell envelope. *Cold Spring Harbor Perspect. Biol.* **2010**, *2* (5), a000414.

(14) Dias, C.; Rauter, A. P. Membrane-targeting antibiotics: recent developments outside the peptide space. *Future Med. Chem.* **2019**, *11* (3), 211−228.

(15) Behuria, H.; Pal, N.; Munda, R.; Sahu, S. Preparation of Giant Unilamellar Vesicles (GUVS) from Bacterial Polar Lipid Extract: Developing a Prokaryotic Model Membrane System. *Biotechnology for sustainable utilization of Bioresources*, Astral International Pvt. Ltd, 2020, pp. 309−320.

(16) Yoon, B. K.; Jackman, J. A.; Valle-González, E. R.; Cho, N.-J. Antibacterial Free Fatty Acids and Monoglycerides: Biological Activities, Experimental Testing, and Therapeutic Applications. *Int. J. Mol. Sci.* **2018**, *19* (4), 1114.

(17) Krok, E.; Stephan, M.; Dimova, R.; Piatkowski, L. Tunable biomimetic bacterial membranes from binary and ternary lipid mixtures and their application in antimicrobial testing. *Biochimica. Biophys. Acta − Biomembr.* **2023**, *1865* (7), 184194.
(18) Tabaei, S. R.; Choi, J. H.; Haw Zan, G.; Zhdanov, V. P.; Cho, N. J. Solvent-assisted lipid bilayer formation on silicon dioxide and gold. *Langmuir* **2014**, *30* (34), 10363−10373.
(19) Carey, A. B.; Ashenden, A.; Köper, I. Model architectures for bacterial membranes. *Biophys. Rev.* **2022**, *14* (1), 111−143.
(20) Dowhan, W. Molecular basis for membrane phospholipid diversity: why are there so many lipids? *Annu. Rev. Biochem.* **1997**, *66*, 199−232.
(21) Sohlenkamp, C.; Geiger, O. Bacterial membrane lipids: diversity in structures and pathways. *FEMS Microbiol. Rev.* **2016**, *40* (1), 133−159.
(22) Kékicheff, P.; Marčelja, S.; Senden, T. J.; Shubin, V. E. Charge reversal seen in electrical double layer interaction of surfaces immersed in 2: 1 calcium electrolyte. *J. Chem. Phys.* **1993**, *99* (8), 6098−6113.
(23) Mukhina, T.; Hemmerle, A.; Rondelli, V.; Gerelli, Y.; Fragneto, G.; Daillant, J.; Charitat, T. Attractive Interaction between Fully Charged Lipid Bilayers in a Strongly Confined Geometry. *J. Phys. Chem. Lett.* **2019**, *10* (22), 7195−7199.
(24) Tabaei, S. R.; Vafaei, S.; Cho, N.-J. Fabrication of charged membranes by the solvent-assisted lipid bilayer (SALB) formation method on SiO2 and Al2O3. *Phys. Chem. Chem. Phys.* **2015**, *17* (17), 11546−11552.
(25) Tae, H.; Yang, C.; Cho, N.-J. Artificial Cell Membrane Platforms by Solvent-Assisted Lipid Bilayer (SALB) Formation. *Acc. Mater. Res.* **2022**, *3* (12), 1272−1284.
(26) Zheng, C. J.; Yoo, J. S.; Lee, T. G.; Cho, H. Y.; Kim, Y. H.; Kim, W. G. Fatty acid synthesis is a target for antibacterial activity of unsaturated fatty acids. *FEBS Lett.* **2005**, *579* (23), 5157−5162.
(27) Pohl, E. E.; Jovanovic, O. The Role of Phosphatidylethanolamine Adducts in Modification of the Activity of Membrane Proteins under Oxidative Stress. *Molecules* **2019**, *24* (24), 4545.
(28) Togashi, N.; Shiraishi, A.; Nishizaka, M.; Matsuoka, K.; Endo, K.; Hamashima, H.; Inoue, Y. Antibacterial Activity of Long-Chain Fatty Alcohols against Staphylococcus aureus. *Molecules* **2007**, *12* (2), 139−148.
(29) Shin, S.; Tae, H.; Park, S.; Cho, N.-J. Lipid Membrane Remodeling by the Micellar Aggregation of Long-Chain Unsaturated Fatty Acids for Sustainable Antimicrobial Strategies. *Int. J. Mol. Sci.* **2023**, *24* (11), 9639.
(30) Di Leone, S.; Kyropoulou, M.; Köchlin, J.; Wehr, R.; Meier, W. P.; Palivan, C. G. Tailoring a Solvent-Assisted Method for Solid-Supported Hybrid Lipid−Polymer Membranes. *Langmuir* **2022**, *38* (21), 6561−6570.
(31) Dixon, M. C. Quartz crystal microbalance with dissipation monitoring: enabling real-time characterization of biological materials and their interactions. *J. Biomol. Technol.* **2008**, *19* (3), 151−158.
(32) Jönsson, P.; Jonsson, M. P.; Tegenfeldt, J. O.; Höök, F. A Method Improving the Accuracy of Fluorescence Recovery after Photobleaching Analysis. *Biophy. J.* **2008**, *95* (11), 5334−5348.
(33) Baba, T.; Takeuchi, F.; Kuroda, M.; Yuzawa, H.; Aoki, K.-I.; Oguchi, A.; Nagai, Y.; Iwama, N.; Asano, K.; Naimi, T.; et al. Genome and virulence determinants of high virulence community-acquired MRSA. *Lancet* **2002**, *359* (9320), 1819−1827.
(34) Heo, H. Y.; Zou, G.; Baek, S.; Kim, J.-S.; Mylonakis, E.; Ausubel, F. M.; Gao, H.; Kim, W. A Methylazanediyl Bisacetamide Derivative Sensitizes Staphylococcus aureus Persisters to a Combination of Gentamicin And Daptomycin. *Adv. Sci.* **2024**, *11* (9), 2306112.
(35) Mangoni, M. L.; Shai, Y. Short native antimicrobial peptides and engineered ultrashort lipopeptides: similarities and differences in cell specificities and modes of action. *Cell. Mol. Life Sci.* **2011**, *68* (13), 2267−2280.
(36) Matsuzaki, K. Why and how are peptide-lipid interactions utilized for self-defense? Magainins and tachyplesins as archetypes. *Biochim. Biophys. Acta* **1999**, *1462* (1−2), 1−10.
(37) Zasloff, M. Antimicrobial peptides of multicellular organisms. *Nature* **2002**, *415* (6870), 389−395.
(38) Perry, W. J.; Grunenwald, C. M.; Van de Plas, R.; Witten, J. C.; Martin, D. R.; Apte, S. S.; Cassat, J. E.; Pettersson, G. B.; Caprioli, R. M.; Skaar, E. P.; et al. Visualizing Staphylococcus aureus pathogenic membrane modification within the host infection environment by multimodal imaging mass spectrometry. *Cell Chem. Biol.* **2022**, *29* (7), 1209−1217.e4.
(39) Kilelee, E. M.; Pokorny, A.; Yeaman, M. R.; Bayer, A. S. Lysyl-Phosphatidylglycerol Attenuates Membrane Perturbation Rather Than Surface Association of the Cationic Antimicrobial Peptide 6w-Rp-1 in a Model Membrane System: Implications for Daptomycin Resistance. *Antimicrob. Agents Chemother.* **2010**, *54* (10), 4476−4479.
(40) Poger, D.; Pöyry, S.; Mark, A. E. Could Cardiolipin Protect Membranes against the Action of Certain Antimicrobial Peptides? Aurein 1.2, a Case Study. *ACS Omega* **2018**, *3* (12), 16453−16464.
(41) Peschel, A.; Otto, M.; Jack, R. W.; Kalbacher, H.; Jung, G.; Götz, F. Inactivation of the dlt operon in Staphylococcus aureus confers sensitivity to defensins, protegrins, and other antimicrobial peptides. *J. Biol. Chem.* **1999**, *274* (13), 8405−8410.
(42) Nagamachi, E.; Kariyama, R.; Kanemasa, Y. The effect of head group structure on phase transition of phospholipid membranes as determined by differential scanning calorimetry. *Physiol. Chem. Phys. Med. NMR* **1985**, *17* (3), 255−260.
(43) Danner, S.; Pabst, G.; Lohner, K.; Hickel, A. Structure and thermotropic behavior of the Staphylococcus aureus lipid lysyl-dipalmitoylphosphatidylglycerol. *Biophys. J.* **2008**, *94* (6), 2150−2159.
(44) Cho, N. J.; Frank, C. W.; Kasemo, B.; Höök, F. Quartz crystal microbalance with dissipation monitoring of supported lipid bilayers on various substrates. *Nat. Protoc.* **2010**, *5* (6), 1096−1106.
(45) Lind, T. K.; Wacklin, H.; Schiller, J.; Moulin, M.; Haertlein, M.; Pomorski, T. G.; Cárdenas, M. Formation and Characterization of Supported Lipid Bilayers Composed of Hydrogenated and Deuterated *Escherichia coli* Lipids. *PLoS One* **2015**, *10* (12), No. e0144671.
(46) Przybylo, M.; Sýkora, J.; Humpolíckova, J.; Benda, A.; Zan, A.; Hof, M. Lipid diffusion in giant unilamellar vesicles is more than 2 times faster than in supported phospholipid bilayers under identical conditions. *Langmuir* **2006**, *22* (22), 9096−9099.
(47) Wilson, B. A.; Ramanathan, A.; Lopez, C. F. Cardiolipin-Dependent Properties of Model Mitochondrial Membranes from Molecular Simulations. *Biophys. J.* **2019**, *117* (3), 429−444.
(48) Flynn, K. R.; Martin, L. L.; Ackland, M. L.; Torriero, A. A. Real-Time Quartz Crystal Microbalance Monitoring of Free Docosahexaenoic Acid Interactions with Supported Lipid Bilayers. *Langmuir* **2016**, *32* (45), 11717−11727.
(49) Pashkovskaya, A. A.; Vazdar, M.; Zimmermann, L.; Jovanovic, O.; Pohl, P.; Pohl, E. E. Mechanism of Long-Chain Free Fatty Acid Protonation at the Membrane-Water Interface. *Biophys. J.* **2018**, *114* (9), 2142−2151.
(50) Kim, S. M.; Zou, G.; Kim, H.; Kang, M.; Ahn, S.; Heo, H. Y.; Kim, J. S.; Lim, K. M.; Ausubel, F. M.; Mylonakis, E.; et al. Antimicrobial activity of the membrane-active compound nTZDpa is enhanced at low pH. *Biomed. Pharmacother.* **2022**, *150*, 112977.
(51) Janke, J. J.; Bennett, W. F. D.; Tieleman, D. P. Oleic Acid Phase Behavior from Molecular Dynamics Simulations. *Langmuir* **2014**, *30* (35), 10661−10667.
(52) Kalyanasundaram, K.; Thomas, J. K. Environmental effects on vibronic band intensities in pyrene monomer fluorescence and their application in studies of micellar systems. *J. Am. Chem. Soc.* **1977**, *99* (7), 2039−2044.
(53) Kalyanasundaram, K.; Thomas, J. K. Solvent-dependent fluorescence of pyrene-3-carboxaldehyde and its applications in the estimation of polarity at micelle-water interfaces. *J. Phys. Chem.* **1977**, *81* (23), 2176−2180.
(54) Ting, H.-C.; Chen, L.-T.; Chen, J.-Y.; Huang, Y.-L.; Xin, R.-C.; Chan, J.-F.; Hsu, Y.-H.-H. Double bonds of unsaturated fatty acids differentially regulate mitochondrial cardiolipin remodeling. *Lipids Health Dis.* **2019**, *18* (1), 53.

https://doi.org/10.1021/acsami.4c11158
ACS Appl. Mater. Interfaces 2024, 16, 56705−56717

(55) Lackinger, M.; Heckl, W. M. Carboxylic acids: versatile building blocks and mediators for two-dimensional supramolecular self-assembly. *Langmuir* **2009**, *25* (19), 11307−11321.
(56) Hong, Y.; Zeng, J.; Wang, X.; Drlica, K.; Zhao, X. Post-Stress Bacterial Cell Death Mediated by Reactive Oxygen Species. *Proc. Natl. Acad. Sci. U. S. A.* **2019**, *116* (20), 10064−10071.
(57) Wong, W. F.; Santiago, M. Microbial Approaches for Targeting Antibiotic-resistant Bacteria. *Microb. Biotechnol.* **2017**, *10* (5), 1047−1053.
(58) Lunde, C. S.; Hartouni, S. R.; Janc, J. W.; Mammen, M.; Humphrey, P. P. A.; Benton, B. M. Telavancin Disrupts the Functional Integrity of the Bacterial Membrane Through Targeted Interaction With the Cell Wall Precursor Lipid II. *Antimicrob. Agents Chemother.* **2009**, *53* (8), 3375−3383.
(59) Lee, H.-J.; Hwang, J. S.; Lee, D. G. Periplanetasin-2 Enhances the Antibacterial Properties of Vancomycin or Chloramphenicol in *Escherichia Coli*. *J. Microbiol. Biotechnol.* **2021**, *31* (2), 189−196.

https://doi.org/10.1021/acsami.4c11158
ACS Appl. Mater. Interfaces 2024, 16, 56705−56717